Nuclear Materials and Energy 9 (2016) 29–35

Contents lists available at ScienceDirect

Nuclear Materials and Energy

journal homepage: www.elsevier.com/locate/nme

Simulation of neutron irradiation damage in tungsten using higher energy protons

R. Rayaprolu[a,*], S. Möller[a], Ch. Linsmeier[a], S. Spellerberg[b]

[a] Forschungszentrum Jülich, Institut für Energie- und Klimaforschung - Plasmaphysik, Partner of the Trilateral Euregio Cluster (TEC), 52425 Jülich, Germany
[b] Forschungszentrum Jülich GmbH, Institut für Neurowissenschaften und Medizin - Nuklearchemie, 52425 Jülich GmbH, Germany

ARTICLE INFO

Keywords:
Irradiation damage
Neutron damage
Fusion
Tungsten
Proton irradiation
Plasma-facing materials

ABSTRACT

This study combines both transmutational changes and accelerated damage by simulation of irradiating tungsten with 16, 30 and 45 MeV protons. Comparative results indicate 30 MeV to be most optimal amongst the three, for uniformity of combined damage. Finally, the results were compared against fission reactor calculations and DEMO relevant compositional changes. Using 30 MeV protons, for damages of 1 dpa equivalent, the rhenium content is calculated as 401 appm. This compares well against appm induced within a DEMO reactor and is better than estimated 50,000 appm for a fission reactor. Using higher energy protons, the recoils are expected to behave similar to neutron displacement damage creation. Additionally, the study suggests near constant and comparable damage for sample thickness's upto 500 µm.

1. Introduction

The damage and degradation of plasma facing components (PFC's), in a fusion reactor environment, is an extensive field of study. Given the wide neutron energy spectrum and simultaneous impact of plasma and photons on PFC's, a study of damage evolution is required to determine the transformation of material characteristics and subsequently the lifetime of PFC's.

Unavailability of high flux ($\geq 10^{14} \frac{n}{cm^2 s}$ [1]) fusion neutron spectrum led to the simulation of irradiation damage by using fission reactors or accelerator systems. Presently, fission reactors and ion irradiation are used for material damage using complementary approaches of compositional changes and displacement damage. Irradiation in fission reactors subjects the samples to neutrons, which is not necessarily the closest approximation to nuclear fusion conditions. The larger thermal neutron flux provides misleading, biased results in terms of (n,γ) transmutations [4] and lower energy recoils compared to fusion conditions. Additionally, long irradiation periods are necessary to achieve the required conditions in a fission environment.

16 MeV protons are known to closely simulate displacement effects produced by 14 MeV neutrons [8]. Further studies highlight the potential of proton irradiation through scattering, damage cross-section and PKA spectra investigations [9,10]. Recent experiments [11,13,15] and feasibility studies [12,14], underline the potential of proton irradiation towards neutron damage investigations. However, in the case of accelerator induced damage creation, no nuclear reactions are currently investigated [5]. This leads to incomplete damage evaluation, as the concerns of micro-structural changes due to transmutated element ingrowth are not addressed. Further, by neglecting the nuclear reactions in accelerator damage studies, the damage through hydrogen and helium are undermined to a large extent and remain unstudied. Thus, a complete consideration of all damage effect of proton irradiation and their exploitation would support the study of macroscopic/engineering parameters for fusion applications.

Significant advances in accelerators have led to higher precision, energy and beam currents, thus serving as a device for multifold applications such as radio-isotope production, damage evaluation and solid state physics experiments, leading to a generally good availability of relevant devices. Additionally, planning an experiment at an accelerator invokes substantially less operational costs, setup time and safety measures compared to fission reactor experiments. The present work evaluates, damage induced by ion beam irradiation, in particular higher energy (16, 30 and 45 MeV) protons. The focus is to damage compared to that of a fusion

* Corresponding author.
E-mail addresses: r.rayaprolu@fz-juelich.de (R. Rayaprolu), s.moeller@fz-juelich.de (S. Möller), ch.linsmeier@fz-juelich.de (Ch. Linsmeier), s.spellerberg@fz-juelich.de (S. Spellerberg).

http://dx.doi.org/10.1016/j.nme.2016.09.008

Table 1
Accelerator facilities at Forschungszentrum Jülich.

Energy (MeV)	Maximum current(μA)	Beam species
16	20	Protons
30	350, 50 and 50	Protons, deuteron's and alphas
45	1 and 1	Protons and deuteron's

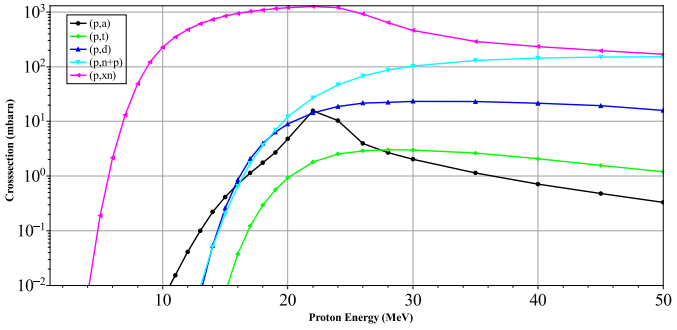

Fig. 1. Major proton cross-sections for ^{186}W up to 50 MeV [17]. At 30 MeV proton energy all partial cross-sections are above 1 mbarn. The reaction channel (p,xn) has the highest cross-section and leads to formation of Re isotopes. Hydrogen and helium are also formed as proton and alpha particle emissions from (p,n+p) and (p,a) reactions respectively.

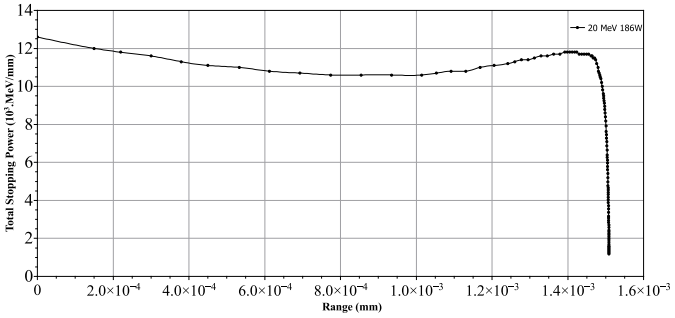

(a) Energy loss of 20 MeV, ^{186}W on natural tungsten

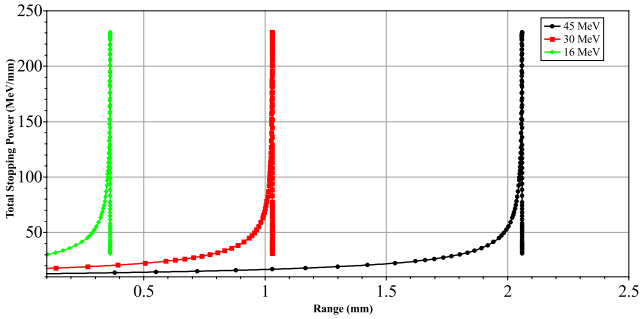

(b) Bragg peak for 16, 30 and 45 MeV proton irradiation on natural tungsten

Fig. 2. Total stopping power V/s Range [20]. Protons have higher depth of penetration as compared to heavy ions. A stable plateau region before the rapid rise of stopping power nearing to Bragg peak is seen in protons. This plateau is considered as the range for homogeneous scattering damage, 300 µm, 500 µm and 1 mm for 16, 30 and 45 MeV protons respectively.

reactor at accelerated rates. This study is restricted to incident proton energies of 16, 30 and 45 MeV, given the possibility of actual exposures for tungsten samples at the operational 16 MeV [27] and 45 MeV [28] or under construction 30 MeV (IBA cyclone 30) cyclotron in Forschungszentrum Jülich (see Table 1). The considerations can in principle be generalized to arbitrary ion beams and energies, but this requires substantial code development beyond the scope of this work.

In view of the primary knock-on atom (PKA) energy distribution [3], it is crucial not to simplify to a single energy. Hence, the damage produced cannot be satisfactorily expressed by dpa numbers, as it cannot account for defect recombination, transmutational changes or heterogeneity of damage. Thereby, the methodology of this study is to emulate the neutron behaviour, while utilising dpa as a comparison factor and not a damage accumulation number. Displacement damage was calculated using the SDTrim.SP 5.07 [18] code, while the nuclear reactions were calculated analytically and compared to neutron results. It is calculated that, in comparison to the fission reactor irradiations, 30 MeV protons on tungsten provide a closer approximation to DEMO fusion reactor damage calculations.

2. Methodology & results

Interaction of protons with tungsten nuclei are governed by screened-Rutherford, classical Rutherford or nuclear forces. For proton energies of consideration (16, 30 and 45 MeV) within this work, the interaction can be defined by a Coulomb potential [7, p. 31–38]. The resulting PKAs' generated through elastic scattering are identical to those induced through neutrons of same energy scattering at the same angle, due to similar masses [8]. Also, the Rutherford cross-section is inversely proportional to square of incident energy, the predominant scattering process is small for the proton energies of consideration.

The nuclear reactions probabilities are expressed as reaction (partial) cross-sections. The major partial cross-sections for protons upto 50 MeV energy on ^{186}W are shown in Fig. 1. For most reaction channels, a rise is noted above 16 MeV proton irradiations. The (p,xn) reactions on tungsten lead to production of rhenium isotopes. Similarly (p,n+p) and (p,a) reactions on tungsten, produce isotopes of tungsten and tantalum with particle emissions of hydrogen and helium respectively. Analogously rhenium, hydrogen and helium are the most investigated damage constituents towards micro-structure and void formation properties for neutron irradiated tungsten[4,5,22,23]. Hence, proton irradiations with 16 MeV or higher energies, exhibit the ability of introducing similar compositional changes as neutron irradiation of tungsten.

Given the similar elastic scattering kinematics, suppressed Rutherford interactions and comparable nuclear reaction products as neutrons on tungsten, the adoption of 16 MeV and higher energy proton irradiations is applied towards comprehension of neutron damage evolution through combination of displacement and transmutational reactions. The displacement damage simulations were generated using SDTrim.SP [18], which provides PKA and secondary knock on atom (SKA) numbers. The nuclear reactions were analytically calculated with TENDL-2015 cross-sections. In the end the cumulative results were compared to fusion neutron damage data [1] and fission irradiation data [2].

2.1. Range of ion irradiation

Ions lose energy quickly when passing matter due to electronic energy loss. The normal practice for heavy ion irradiation damage study is to select energies producing the Bragg peak at the desired location of investigation within the sample (1–10 µm) to achieve maximum damage rate. Fig. 2(a) depicts the stopping power loss over energy for a 20 MeV ^{186}W irradiation on natural tungsten sample with a Bragg peak at ~1.5 µm. For thick samples, the damage profile of heavy ion irradiation is inhomogeneous as the collision probability is not constant throughout the depth with the strongest variation at the Bragg peak. Light ions such as protons display much higher homogeneous range of damage [16], varying from 10 µm to several mm, depending on the energy. Fig 2(b) displays the stopping power loss over range for 16, 30 and 45 MeV

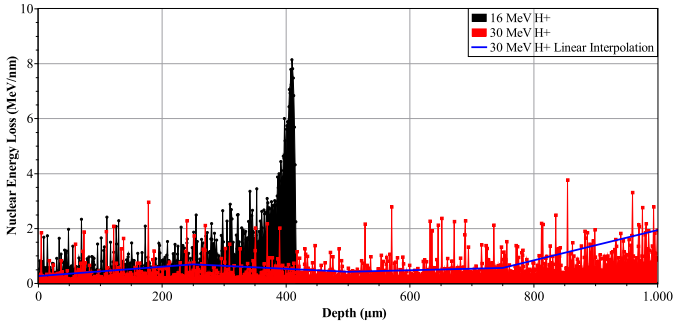

Fig. 3. Scattering losses (Nuclear Energy Loss $>E_d$) over tungsten sample depth upto 1 mm. Near constant nuclear energy loss for 30 MeV protons on tungsten is seen till 500 μm in contrast to 16 MeV proton which displays the characteristic Bragg's peak from 300 μm.

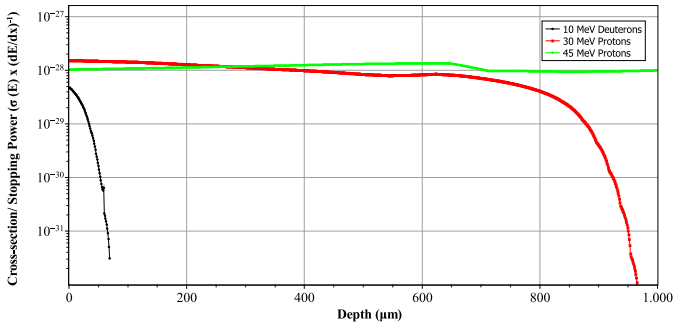

Fig. 4. Nuclear reaction cross-section sum variation over tungsten sample depth for 10 MeV deuteron, 30 and 45 MeV protons.

protons. It is clearly seen that, as the proton energy increases from 16 to 30 and 45 MeV, there is Bragg peak shift from ~360 μm to higher depths of ~1.03 mm and ~2.06 mm respectively. In view of the higher penetration range of protons and rapid rise of stopping power close to the Bragg peak, the plateau region prior to the Bragg peak, which is devoid of rapid drop in proton energy, is considered in this work as applicable irradiation range. This results in an applicable initial sample thickness of 300 μm, 500 μm and 1 mm for 16, 30 and 45 MeV protons respectively. This strategy is important for all irradiation damage types as it considers variations of nuclear reaction probabilities and PKA distribution, both closely related to the beam energy.

The determination of applicable range is based on both the scattering and nuclear reactions homogeneity of damage over the depth of irradiation and hence both are considered separately. SDTrim.SP provides the nuclear energy loss greater than E_d, which for 30 MeV protons is plotted in red in Fig. 3. Additionally for comparison, 16 MeV proton energy loss greater than E_d is also shown. Although the range is over 400 μm, the applicable range is limited to ~300 μm, after which the Bragg peak take over. Similarly, the range for 30 MeV protons is above 1 mm, but above 800 μm the energy loss starts to increase and limits the range of homogeneous scattering damage. The noisy behaviour is the result of statistical error through monte-carlo method and for averaging, a 5 point linear interpolation is additionally shown for 30 MeV protons.

For the consistency in nuclear reactions, the reaction rate is defined by the product of cross-section times the inverse of the stopping power (Eq. (5)). This term is summed up for all reaction channels and the variation is plotted along the depth of sample in Fig. 4. It includes the change in energy and in turn variation of cross-section over depth of the sample. It is evident from Fig. 4, that the nuclear reaction rates stay within a factor of two until 500 μm as compared to a sharp drop within the 50 μm for 10 MeV

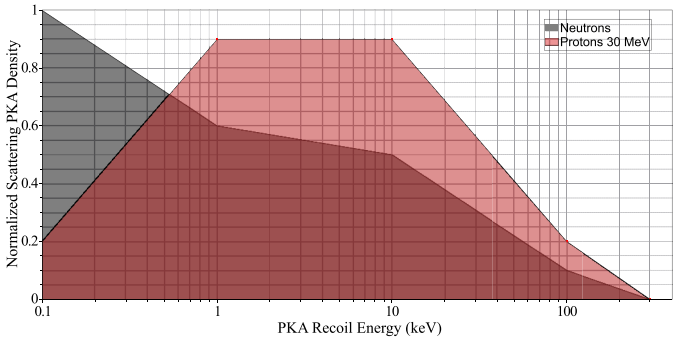

Fig. 5. Normalized scattering PKA energy distribution of 30 MeV protons and DEMO neutrons on tungsten. Using SRIM, it is noticed, 30 MeV protons can achieve greater part of high energy recoils than DEMO neutrons.

deuteron. The energy drop for 30 MeV protons within 500 μm is 9.9 MeV, above which the stopping power increases and cross-sections drop. For 45 MeV, the nuclear reaction rates remain constant over the entire range of 1 mm, within a factor of two.

Combining the scattering and nuclear reaction variation through depth, it is seen that the practical viability of 30 MeV for damage studies is about 500 μm. This is 500x above the standard ranges practised for heavy ion accelerator damage samples and opens a path to studies of macroscopic samples and parameters. Fission reactor studies are often using sample thickness's in the same order, allowing direct comparisons.

2.2. Displacement damage

The primary knock on atom (PKA) spectrum and subsequent cascade development is known to induce irradiation hardening, increase of yield stress, void formation, swelling and segregation of 'He' atoms to grain boundaries [25]. The recoil energies are a major factor as the growth of damage cascades within the sample is governed by the quantity, energy distribution and type (mass and charge) of primary knock ons'. In fact, different initial PKA energies are found to initiate different cascade dimensions and cluster dynamics [24], leading also to different survival rates of frenkel pairs (true dpa). Previous studies of 10–20 MeV protons on 'Fe', 'Cu', 'Nb' and 'Au' [9,10] clearly indicate good reproduction of recoil distributions for recoil energies greater than few keV. With the consideration of 500 μm sample thickness for 30 MeV protons, the exit energy of protons (see Table 2) is still enough to avoid low energy recoil production.

For the above energies, using coulomb potential to illustrate Rutherford scattering, Table 2 suggests theoretically the maximum and average PKA recoil energies, where the incoming proton PKA and outgoing proton PKA are mentioned. The average PKA energy (T_{avg}) was estimated using a minimum of 90 eV for displacement threshold energy (E_d) of tungsten substituted within Eq. (1) [7]. T_{max} refers to maximum PKA energy.

$$T_{avg} = E_d \times ln\left(\frac{T_{max}}{E_d}\right) \quad (1)$$

For 30 MeV protons, the energy lost to recoils is seen to vary between 5 eV to 120 keV as calculated by SRIM [21]. A normalized plot of the energy lost to recoils compared against that of 14 MeV or DEMO spectrum neutrons is displayed in Fig. 5. The energy distribution is started from 90 eV, which is the displacement threshold energy for tungsten. It is observed that the range of PKA energies obtained from neutron scattering are also produced by proton scattering. The neutrons have greater proportion of low energy recoils than protons.

Table 2
Maximum & average PKA energies for protons on tungsten with E_d = 90 eV. Energy drop on 300, 500 and 1000 μm W.

Incident Proton Energy (MeV)	Incident Proton PKA E_max (keV)	Incident Proton PKA E_avg (eV)	Sample Thickness (μm)	Energy Loss (MeV)	Outgoing Proton Energy (MeV)	Outgoing Proton PKA E_max (keV)	Outgoing Proton PKA E_avg (eV)
45	968	836	1000	14.7	30.3	651	800
30	646	799	500	9.9	20.1	432	763
16	344	742	300	11.3	4.7	101	632

Table 3
SDTrim calculation results for protons on tungsten run for 10^5 particles.

Proton energy	45 MeV	30 MeV (1mm)	30 MeV (500 μm)	16 MeV
PKA/proton > E_d	3.5	7.2	2.6	3.4
SKA/proton > E_d	13.6	29.4	10	13.1
total knock on atoms	871	1826	641	833
damage cross-section	1.7×10^{-21}	3.6×10^{-21}	2.5×10^{-21}	5.5×10^{-21}
dpa/s @ 1 μA/cm^2	1.1×10^{-8}	2.3×10^{-8}	1.6×10^{-8}	3.4×10^{-8}

In a thermal fission reactor ($^{235}_{92}$U), 5 MeV of energy is released in the form of prompt neutrons for every fission event, wherein, the most likely neutron energy is 0.7 MeV [26, p. 10–11]. 0.7 MeV relates to maximum energy transfer to a tungsten PKA of 15 keV. Results from Table 2 indicate a closer approximation of maximum PKA energy of 303 keV of DEMO 14 MeV neutron scattering on tungsten by using 16 and 30 MeV protons. The average PKA energy for tungsten in DEMO, excluding the contribution of light ions, is reported as 3.2 keV, while for fission reactors (HFIR) it is around 1 keV [6]. With the limitation of 500 μm as sample depth for 30 MeV protons, they display average PKA values between 0.8 - 0.76 keV between entry to exit. In conclusion, both fission and proton induced PKA spectra provide similar, but slightly lower average PKA energies than expected for DEMO.

SDTrim.SP 5.07, is adapted to handle high energies of incoming projectiles by use of the Ziegler - Biersack stopping power model for inelastic stopping [21]. SDTrim.SP 5.07 was initiated for each proton energy to obtain the PKA, SKA (secondary knock on atoms) and total knock on atoms. In the interest of comparison with 45 MeV, 30 MeV protons computations were repeated for 1 mm range additionally. The number of histories was 10^5 particles, while the displacement energy for tungsten was 90 eV[19]. Beam direction was considered normal to the target surface and the surface binding energy was assumed as 1 MeV to avoid sputtering reactions slow down calculations. Output generated by SDTrim.SP yields a damage number (N_{DAM}), from which the damage cross-section and dpa was calculated using Eqs. (2) and (3). The values of Δ, N_P, ρ, A, N_A and ϕ correspond to depth interval, number of virtual projectiles, density, area, number of target atoms and fluence respectively. The PKAs' and SKAs' per proton >E_d, total knock on atoms, damage cross-section and dpa estimation are shown in Table 3.

$$Damage\ Crosssection(\sigma) = \frac{N_{DAM}A}{N_A N_P} \tag{2}$$

$$DPA = \frac{\frac{N_{DAM}}{\Delta N_P}}{\rho} \times \phi \tag{3}$$

Comparing PKA and SKA > E_d values for 16, 30 (500 μm) and 45 MeV with constrained ranges in Table 3, we observe similarities of cascade development. In contrast the 30 MeV (1 mm) displays a much higher number of PKA, SKA and total knock on atoms. This is due to the higher number of low energy recoils which occur close to the Bragg peak. Also evident from the damage cross-sections listed in Table 3, is the increase in scattering interactions with lowering of projectile energy, but at the cost of decrease in high energy scatterings.

2.3. Nuclear reactions

Activation and transmutation products are an important part of the fusion material qualification requirements. Given the wide energy flux spectrum of fusion neutrons, the transmutation products are calculated by folding the differential cross-sections with the neutron energy spectrum through use of programs such as FISPACT/EASY. The programs require users to input composition, mass and irradiation parameters [1].

Protons lose energy upon passage through materials. For calculating the nuclear reactions, the differential cross-sections are folded with inverse of the stopping power (Eqs. (4) and (5)). As the proton energy drop is limited to 20 MeV and a single element ('W') was investigated, the proton calculations were made analytically with TENDL-2015 [17] cross-sections and the basic Bethe-Bloch equation. Mother-daughter decay relationships were derived and included in the analytical calculations. The activity immediately after irradiation and specific cooling times were calculated from which the number of transmutated atoms and subsequently appm were obtained.

In Eq. (4), 'v' and 'ze' are the velocity and charge of the primary particle (protons), while 'N' and 'Z' are the number density and atomic number of the absorber atoms (tungsten atoms). 'm_0' and 'e' represents the electron rest mass and charge respectively. For sample thickness of consideration (0.3–1 mm), the stopping power predicted by Eq. (3), was compared against that calculated by SRIM [20] which held within a difference of 2%.

$$-\frac{dE}{dx} = \frac{4\pi e^4 z^2}{m_0 v^2} NB \tag{4}$$

Relevant differential cross-sections above 1 mbarn between 5 - 50 MeV proton energy were compiled for 180, 182, 183, 184 and 186 W from TENDL-2015 database[17] with reactions considered listed in Table 4. Together, the stopping power and reaction cross-sections were incorporated in Eq. (5), to obtain the reaction rates and activities of produced nuclei, where N_T is the number of tungsten target atoms, H is the isotopic abundance, I_P is the projectile current, λ is the half life constant, E_1 is the beam energy and its gradual decrease through the sample results in exit energy E_2.

$$A = N_T H I_P (1 - e^{-\lambda t_{irr}}) \int_{E_1}^{E_2} \left[\frac{dE}{dx}\right]^{-1} \sigma(E) dE \tag{5}$$

The above equation can be rewritten in terms of reaction rate for decay equations as follows.

$$A = R(1 - e^{-\lambda t_{irr}}) \tag{6}$$

The mother daughter relations were introduced as described in Eqs. (7)–(9), for a sample having N_1 stable atoms at the start of

Table 4
List of reactions considered for nuclear reaction calculations obtained from TENDL-2015[17].

180 W	182 W	183 W	184 W	186 W
p,2n	p,3n	p,3n	p,3n level 0	p,3n level 0
p,3n	p,2n	p,n	p,2n	p,3n level 5
p,n	p,n level 0	p,2n level 0	p,3n level 2	p,2n
p,n+p level 0	p,n+p	p, n+ p	p, n level 5	p,n+p level 6
p,d level 0	p,n level 2	p,2n level 2	p, n level 0	p,n level 4
p,a	p,d	p,d	p,n+p level 0	p,n+p level 0
p,2n+p	p,a	p,n + a	p,n+p level 7	p,n level 0
p,n+a	p,2n+p	p,2n+p	p,d level 0	p,d level 6
p,n+p level 2	p,n+a level 0	p,a level 2	p, d level 7	p,2n+p
p,n+d	p,n+d	p,a level 0	p,a	p,a
p,d level 2	p,t	p,n+d	p,2n+p	p,d level 0
p,t	p,n+a level 1	p,t	p,n+a level 2	p,n+d
p,2n+a	p,2n+a	p,n+t	p,n+d	p,n+a level 29
p,g	p,n+t level 0	p,2n +a level 0	p,n+a level 0	p,n+a level 1
p,n+t	p,g	p,g level 0	p,t	p,t
p,2p	p,2p	p,2n +a level 1	p,n+t	p,n+a level 0
p,3He level 0	p,3He level 0	p,g level 5	p,2n+a	p,n+t level 0
p,3He level 1	p,n+t level 2	p,3He	p,g	p,2n+a
p,3n+p	p,3He level 2	p,3n + a	p,2p	p,n+t level 7
p,2n+d	p,3n+a	p,3n + p	p,2n+d	p,g
p,n+2p level 0	p,3n+p level 0	p, 2p level 0	p,3n+p	p,3n+p level 0
p,n+2p level 1	p,2n+d level 0	p, 2p level 1	p,3n+a level 0	p,2n+d level 0
p,2n+t	p,3n+p level 2	p, 2n+d	p,2n+t	p, 3He
	p,2n+d level 2	p, 2p level 29	p,3n+a level 1	p,3n+p level 7
	p,2n+t	p,2n+t level 0	p,n+3He	p,2n+d level 7
	p,n+2p level 0	p, n+ 3He level 2	p,n+2p level 0	p,2n+t
	p,n+2p level 2	p, n+ 2p	p,n+2p level 1	p,2p
		p,n + 3He level 0	p,n+2p level 29	p,3n+a level 2
		p,2n+t level 2	p,3n+d	p,3n+a level 0
				p,n+3He
				p,n+2p
				p,3n+d
				p,3n+t

irradiation and producing N_2 atoms during irradiation and so forth as per the sequence below.

$$N_{1(stable)} \rightarrow N_2 \xrightarrow{\lambda_2} N_3 \xrightarrow{\lambda_3} N_4 \xrightarrow{\lambda_4}$$
$$A_{1(stable)} \rightarrow A_2 \xrightarrow{\lambda_2} A_3 \xrightarrow{\lambda_3} A_4 \xrightarrow{\lambda_4}$$

$$N_2(t) = \frac{R}{\lambda_2}(1 - e^{-\lambda_2 t}) \tag{7}$$

$$N_3(t) = R\left[\frac{1}{\lambda_3}(1 - e^{-\lambda_3 t}) + \frac{1}{\lambda_2 - \lambda_3}(e^{-\lambda_2 t} - e^{-\lambda_3 t})\right] \tag{8}$$

$$N_4(t) = R\left[\frac{1}{\lambda_4}(1 - e^{-\lambda_4 t}) + \frac{1}{\lambda_3 - \lambda_4}(e^{-\lambda_3 t} - e^{-\lambda_4 t}) + \frac{\lambda_3}{\lambda_3 - \lambda_2}\left(\frac{e^{-\lambda_4 t} - e^{-\lambda_2 t}}{\lambda_4 - \lambda_2} + \frac{e^{-\lambda_4 t} - e^{-\lambda_3 t}}{\lambda_4 - \lambda_3}\right)\right] \tag{9}$$

Similar equations were derived for the decay during post irradiation cooling time. As the area and depth of beam irradiation are considered within the activation equation, straightforward ppm calculations were performed using atomic density of 6.305×10^{22} cm^{-3} for the tungsten sample.

2.4. Comparison of irradiation options

The heavy transmutation reaction products (Re, Os, Ta...), are grouped under a single term for their similar damage threshold energies. Similarly the light transmutational reaction products are grouped together on account of e.g. their void/ bubble formation tendencies.

To analyse, the results were partitioned to three major subdivisions of:

Table 5
Ratio of proton reaction products to DEMO neutron reaction products from tungsten irradiation.

Ratio to DEMO neutrons	45 MeV Protons / DEMO neutrons	30 MeV Protons / DEMO neutrons	16 MeV Protons / DEMO neutrons
Heavy Reaction Products	0.8	0.4	0.09
Tungsten (only scattering)	47	34	45
Light Reaction Products	440	135	0.5

1. Heavy Reaction Product PKAs- Tungsten, Rhenium, Tantalum and Hafnium
2. Light Reaction Product PKAs- Protons and alphas
3. Tungsten elastic scattering PKAs

With protons being charged particles, scattering reactions are the predominant damage creation mechanism. When scattering reactions outweigh desired nuclear transmutation products, the simulation of DEMO neutron damage would provide biased, scattering dominated damage production as in the case of heavy ion irradiation. To compare damages, the corresponding ratios' between proton and DEMO neutron induced reactions are listed and examined. The ideal case would be an equal ratio for heavy reaction products, scattering products and light reaction products produced by protons in comparison to DEMO neutrons. This can be interpreted as a ideal acceleration of damage through protons.

Table 5 portrays the actual ratio of heavy reaction products, scattering products and light reaction products of protons to that by DEMO neutrons. Due to cross-sectional differences and higher scattering probability, the scatterings from protons are about 40x of that by neutrons. It is noticed that we can quantitatively introduce heavy reaction products through use of protons. For 30 MeV protons, the heavy reaction products formed are 40% of that from neutrons, this though is at the cost of inducing 135x more light

Table 6
Transmutation comparison for 30 MeV protons and DEMO neutrons on tungsten against 1 dpa displacement damage accumulation.

Production (appm)	30 MeV Protons	DEMO Reactor's First Wall [1]	Fission Reactor [2]
Hydrogen	29	1	0
Helium	7.2	0.5	0
Rhenium	401.5	700	50,000
Tantalum	6.5	50	200
Osmium	0.3	4	2000

products of hydrogen and helium. For 45 MeV proton irradiations, a closer induction of heavy reaction products upto 80% is seen. In contrast, the number of light reaction products is much larger than that produced by 30 MeV protons and DEMO neutrons. For 16 MeV protons, on account of lower reaction cross-sections, both heavy reaction products and light reaction products induced are deficient.

For a deeper insight into the nuclear transmutation product evolution, comparison of a 30 MeV proton irradiated tungsten sample (10 mm dia, 500 μm thickness) against DEMO [1] and fission reactors (PWR & HFR-Petten) [2] is shown in Table 6 for an irradiation of 1 dpa. The concentrations (appm) for DEMO reactor are considered at 6 dpa/ year while for fission reactors at 1 dpa/ year. The heavy products of osmium and rhenium are better approximated through use of 30 MeV protons against fission reactors for the DEMO reactor first wall. Although, the hydrogen and helium produced by 30 MeV proton irradiation is far larger than that produced in a DEMO scenario. THe ratios pf Table 5 of scattering to heavy products turned out to be significantly weakened in the concentration per dpa picture as proton irradiation produces significantly less dpa per scattering compared to 14 MeV neutrons. Fission reactors show high amount of (n,γ) reactions leading to 50,000 appm of 'Re' concentration and very low 'H' and 'He' production. The major reaction channels of neutron interaction (n,γ) and (n,2n) produce excited states of tungsten, formation of rhenium is a through decay of these excited nuclei. The W-Re microstructure formation is thought to induce significant variation of mechanical and physical properties such as hardening and hydrogen retention. Protons lead to direct transmutation of tungsten to rhenium via the (p,xn) reaction channel and can thus lead to similar formation of W-Re micro-structure phase.

2.5. Metal impurity time-evolution after irradiation

Under DEMO neutron flux irradiation of stable 'W' isotopes, (n,γ) and (n,2n) reactions produce unstable radioactive 'W' atoms. These atoms undergo β^- decay into 'Re' and 'Os' isotopes. The decay products with the highest concentrations are $^{185,\ 187}$Re and $^{186,\ 188}$Os. As these isotopes are stable or long lived, the 'Re' concentration does not vary appreciably with time after irradiation. Proton irradiation of 'W' produces 'Re' isotopes as a direct reaction product through (p,xn) reaction channels. Mostly neutron deficient isotopes of 'Re' such as $^{180,\ 181,\ 182,\ 183,\ 184}$Re are produced, which intrinsically are unstable with half lives of minutes to days, decaying to stable isotopes of 'W' and 'Ta' via electron capture or β^+ decay. Thus, varying cooling times leads to variation in atomic concentrations of transmutation elements. Consequently, the post irradiation testing results could differ due to decay.

The change in concentration of heavy elements through decay and ingrowth in proton irradiated tungsten over a cooling time of 1.5 years is depicted in Fig. 6. The calculations have been performed for tungsten sample size of 10 mm diameter, 500 μm thickness, irradiated for 13.17 h at a beam fluence of 16.6 Coulomb and then allowed to cool. The short lived rhenium isotopes, $^{177,\ 178,\ 179,\ 180}$Re decrease over a few hours resulting in sharp ingrowth of tantalum. Remaining rhenium isotopes have half lifes of days, thus slowing down the process reaching a quasi-static situation after about 1 year. This provides an opportunity to understand the influence of rhenium and tantalum in tungsten at various stages through extension of cooling periods.

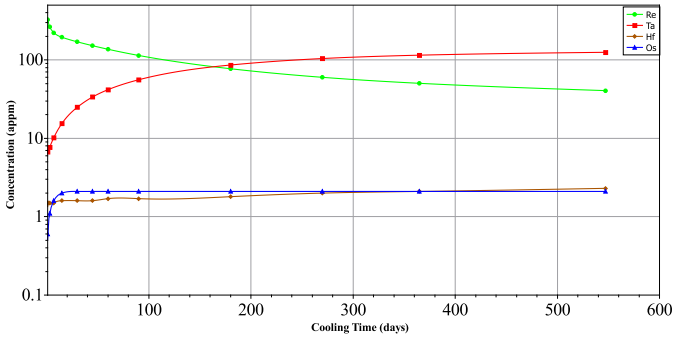

Fig. 6. Decay & ingrowth of heavy elements over time for 30 MeV proton irradiated tungsten.

3. Discussion

The entire approach utilised in this study of using medium(30 MeV) energy protons is not to calculate the damage but more as a tool to investigate the exact nature of primary damage mechanisms and their effects on materials. In view of this, the primary knock ons created by energetic (30 MeV) protons within the sample were simulated. The capability of inducing transmutation effects leading to chemical composition changes were also calculated and compared to those estimated for DEMO neutrons. The chemical compositional changes are assumed to lead to similar microstructural changes as that under DEMO neutron irradiation conditions. The energy of primary knock ons was simulated in order to find out whether the secondary knock ons and cascades initiated would also have similar behaviour to that obtained through DEMO neutrons. Lastly range determination through constancy of scattering and nuclear reaction cross-sections was carried out to obtain a working thickness for sample investigation.

As a technical example of proton irradiation 350 μA are taken as maximum from one of the possible industrial cyclotrons. This can lead to a critical heat load on the sample of about 40 MW/m^2. Definitely higher beam current densities are advantageous for faster irradiation, but the related questions of targetry are out of the scope of this publication.

It was noticed that 30 MeV protons in tungsten have, similar to DEMO spectrum neutrons, more scattering reactions than nuclear transmutations, hence being the dominant effect of damage creation. Also similar transmutation product elements are obtained, but through different reaction mechanisms for protons as for neutrons. The nuclear reactions induced per neutron, are two orders of magnitude higher than those caused per proton for similar damage estimates. The comparison Table 7, displays the capabilities and drawbacks of 30 MeV protons against other irradiation test facilities. Spallation irradiation values quoted are expected numbers for tungsten, as they are derived from considering 4–6 dpa/year at FMITS [29]. The rhenium and hydrogen concentrations for 2 months of exposure to DEMO spectrum neutrons (1 dpa) and similarly 1 dpa of protons is 700 appm, 1 appm and 401 appm, 29 appm respectively. In terms of range, 30 MeV protons are able to provide constant damage upto 500 μm, which is advantageous, as it surpasses the heavy ion damage ranges and is compatible with sample conditions of fission reactors for post ir-

Table 7
Comparison of major factors relating to tungsten irradiation facilities.

Description (for 1 dpa in W)	30 MeV H+ (445 μA/cm^2)	Heavy Ions	Fission (HFR) [2]	Spallation (expected) [29]	DEMO FW [1]
Maximum PKA Energy (keV)	646	$\gg$1000	100	–	303
Time taken	14 h	Hours	1 year		2 months
Thickness Range (μm)	500	1–10	200–4000	200–4000	–
'H' Production (appm)	29	0	0	1	1
'He' Production (appm)	7.2	0	0.01	0.1–0.01	0.5
're' Production (appm)	401	0	50,000	300–500	700

radiation comparison and also suitable for investigation of macroscopic material properties. Additionally, the primary elastic scattering recoil energies of protons on tungsten are seen to be consistent with 14 MeV neutron scattering interactions. A major advantage over fission neutron irradiation is the high energy recoil component which can be seen. This component is not generated during the fission irradiations, as the neutron energies are lower than 5 MeV.

It is seen that 30 MeV protons would provide a solution for DEMO reactor irradiation material damage studies. High activity of samples similar to fission reactor irradiated samples would necessitate the need of hot cells for post irradiation investigations. Spallation sources could also replicate consistent damage but additionally introduce large number of unwanted transmutation products due to the nature of spallation reactions. The planned IFMIF accelerator is designed specifically to obtain the exact neutron spectrum as a DEMO reactor. While the 30 MeV protons wouldn't replicate it point to point, they could be established as a complementary experimental irradiation tool to understand the material properties and mechanical properties in a fast and cost efficient manner.

References

[1] M.R. Gilbert, J.-C. Sublet, R.A. Forrest, Handbook of activation, transmutation, and radiation damage properties of the elements simulated using FISPACT-II & TENDL-2014, Magnetic Fusion Plants,February, vol. CCFE-R(15)26, 2015.

[2] M.R. Gilbert, J.-C. Sublet, Handbook of activation, transmutation, and radiation damage properties of the elements simulated using FISPACT-II & TENDL-2014, Nuclear Fission plants (PWR focus),December, vol. UKAEA-R(15)31, 2015.

[3] M.R. Gilbert, J.-C. Sublet, R.A. Forrest, PKA distributions of the elements simulated using TENDL-2014, Magnetic Fusion Plants CCFE-R(15) (February(26-supplement)) (2015).

[4] M. Fukuda, K. Yabuuchi, S. Nogami, A. Hasegawa, T. Tanaka, Microstructural development of tungsten and tungsten-rhenium alloys due to neutron irradiation in HFIR, J. Nuclear Mater. 455 (2014) 460–463.

[5] S.J. Linke, A. Möslang, Evaluation of irradiation facility options for fusion materials research and development, Fusion Eng. Des. 88 (2013) 472–482.

[6] M.R. Gilbert, J. Marian, J.-C. Sublet, Energy spectra of primary knock-on atoms under neutron irradiation, J. Nuclear Mater. 467 (2015) 121–134.

[7] G.S. Was, Fundamentals of Radiation Material Science - Metals and Alloys, Springer, 2007.

[8] C.M. Logan, J.D. Anderson, A.K. Mukherjee, Proton simulation of displacement effects induced in metals by 14MeV neutrons, J. Nuclear Mater. 48 (1973) 223–232.

[9] A.M. Omar, J.E. Robinson, D.A. Thompson, Calculation of scattering and radiation damage parameters for 14 mev neutrons and 10 to 20 mev protons on fe, ni, cu, nb, and au, J. Nuclear Mater. 64 (1977) 121–129.

[10] D.A. Thompson, A.M. Omar, J.E. Robinson, 10-16 MeV proton irradiation damage in iron and copper, J. Nuclear Mater. 85 & 86 (1979) 509–513.

[11] B.H. Sencer, G.S. Was, M. Sagisaka, Y. Isobe, G.M. Bond, F.A. Garner, Proton irradiation emulation of PWR neutron damage microstructures in solution annealed 304 and cold-worked 316 stainless steels, J. Nuclear Mater. 323 (2003) 18–28.

[12] H. Korkut, T. Korkut, A. Kara, M. Yiğit, E. Tel, Monte carlo simulations of 17.9 - 22.3 MeV energetic proton irradiation effects on bcc zirconium fusionic materials, J. Fusion Energy 35 (2016) 591–596.

[13] Y. Murase, J. Nagakawa, N. Yananoto, Effects of implanted hydrogen on fatigue behavior of F82H under irradiation, J. Nuclear Mater. 417 (2011) 120–123.

[14] E. Abad, R. Martínez-Ballarín, F.J. Bermejo, A feasibility study of a proton irradiation laboratory for fusion materials at ESS-Bilbao, Physics Procedia 60 (2014) 61–65.

[15] S.-H. Chi, J.-H. Hong, Evaluation of irradiation effects of 16 mev proton-irradiated 12Cr-1MoV steel by small punch (SP) tests, Scripta Metallurgica et Materialia 30 (12) (1994) 1521–1525.

[16] C. Abromeit, Aspects of simulation of neutron damage by ion irradiation, J. Nuclear Mater. 216 (1994) 78–96.

[17] A.J. Koning, D. Rochman, J. Kopecky, J.C. Sublet, E. Bauge, S. Hilaire, P. Romain, B. Morillon, H. Duarte, S. van der Marck, S. Pomp, H. Sjostrand, R. Forrest, H. Henriksson, O. Cabellos, S. Goriely, J. Leppanen, H. Leeb, A. Plompen, R. Mills, TENDL-2015: TALYS-based evaluated nuclear data library, https://tendl.web.psi.ch/tendl_2015/tendl2015.html.

[18] W. Eckstein, R. Dohmen, A. Mutzke, R. Schneider, SDTrimSP: A Monte Carlo Code for Calculating Collision Phenomena in Randomized Targets, January 2007.

[19] ASTM E521, 96(2009) Standard practice for neutron irradiation damage simulation by charged particle irradiation.

[20] Nucleonica Nuclear Science Portal (www.nucleonica.com), Version 3.0.49, 2014, Nucleonica GmbH, Karlsruhe, Germany.

[21] J.F. Ziegler, J. Biersack, M.D. Ziegler, The stopping and range of ions in matter, Lulu Press, 2008.

[22] J. Marian, T.L. Hoang, Modelling fast neutron irradiation damage accumulation in tungsten, J. Nuclear Mater. 429 (2012) 293–297.

[23] A. Hasegawa, M. Fukuda, S. Nogami, K. Yabuuchi, Neutron irradiation effects on tungsten materials, Fusion Eng. Des. 89 (2014) 1568–1572.

[24] T. Troev, N. Nankov, T. Yoshiie, Simulation of displacement cascades in tungsten irradiated by fusion neutrons, Nuclear Instruments Methods Phys. Res. B 269 (2011) 566–571.

[25] B.N. Singh, Impacts of damage production and accumulation on materials performance in irradiation environment, J. Nuclear Mater. 258–263 (1998) 18–29.

[26] W.M. Stacey, Nuclear Reactor Physics, 2nd edition, Wiley-VCH Verlag GmbH & Co, 2007.

[27] B. Scholten, S. Spellerberg, W. Bolten, H.H. Coenen, Development of a target system at the baby cyclotron BC1710 for irradiation of solids and gases and the adaptation of existing target systems to the external beamline at the injector of COSY, 13th Workshop on Targetry and Target Chemistry, 2010.

[28] W. Bräutigam, R. Brings, R. Gebel, R. Maier, Status and perspectives of the cyclotron JULIC as COSY injector, NUKLEONIKA 48 (2003) S123–S126.

[29] W. Lu, F.X. Gallmeier, M.W. Wendel, Transmutation products in steel and tungsten samples at FMITS, 12th International Workshop on Spallation Materials Technology, 2014.